Journal of Hydrology 612 (2022) 128154

Contents lists available at ScienceDirect

Journal of Hydrology

journal homepage: www.elsevier.com/locate/jhydrol

Research papers

Amplification of non-stationary drought to heatwave duration and intensity in eastern China: Spatiotemporal pattern and causes

Yaojin Bian [a], Peng Sun [a,*], Qiang Zhang [b,c,*], Ming Luo [d], Ruilin Liu [a]

[a] School of Geography and Tourism, Anhui Normal University, Wuhu, Anhui, China
[b] State Key Laboratory of Earth Surface Processes and Resource Ecology, Beijing Normal University, Beijing 100875, China
[c] Faculty of Geographical Science, Beijing Normal University, Beijing, China
[d] School of Geography and Planning, Guangdong Key Laboratory for Urbanization and Geo-simulation, Guangdong Provincial Engineering Research Center for Public Security and Disaster, Sun Yat-sen University, Guangzhou, China

ARTICLE INFO

This manuscript was handled by Emmanouil Anagnostou, Editor-in-Chief

Keywords:
Heatwaves
Meteorological drought
Compound drought-heatwave events
NSPEI

ABSTRACT

Amplifying the frequency and loss of weather and hydrological extremes under climate warming have aroused increasing human concerns in recent decades and it is particularly the case for compound drought-heatwave (CDH) events. The drought index based on the hypothesis of non-stationarity is of great significance for the study of CDH events. Here we presented spatiotemporal patterns of CDH, general heatwaves (GHW, he heatwave that does not occur in dry months) and relevant circulation backgrounds in eastern China. We found that heatwaves are starting earlier and ending later and later. While, the termination date of heatwaves in southern China is late than those in northern China. Significant increases since the 1980 s were detected in the frequency, duration, and intensity of heatwaves and the frequency of CDH events in eastern China. Besides, heatwaves were observed mainly in the middle and lower Yangtze River basin and in the Sichuan Basin as well. Most areas of eastern China were dominated by higher occurrence probability of CDHs in July and the probability was as high as 0.49. The duration and intensity of the CDHs were 0.28 days longer and 11.14℃ higher than GHWs. Further examinations show that the western Pacific subtropical high (WPSH) has a significant influence on the occurrence of heatwaves. The average position of the WPSH is shifted westward and its intensity is relatively stronger, thus favoring the occurrence of heatwave events. The occurrence of compound events in eastern China cannot be separated from the influence of large-scale circulation and atmospheric changes.

1. Introduction

Global warming will amplify extreme meteorological events and will have profound impacts on socioeconomic development (Gao et al., 2019; Tegegne et al., 2020; Zscheischler et al., 2018). Compared with single extreme event, the impact of compound drought-heatwave (CDH) events is more severe (Leonard et al., 2014; Zhang et al., 2021b). The CDH disasters in Eastern Europe and Russia in 2003, 2010, and 2018 caused considerable mortalities and socioeconomic losses (Liu et al., 2020). CDH events in Europe have resulted in two-fold increase in crop losses over the past 50 years (Bras et al., 2021). Therefore, a thorough understanding of CDH is highly significant for human mitigation to natural hazards in the backdrop of global warming.

A heatwave event is defined as a period with air temperature higher than a certain threshold and synchronous occurrence of drought and heatwave is defined as a CDH event (Kong et al., 2020; Shi et al., 2021; Mukherjee and Mishra, 2020). Drought is usually accompanied by high air temperature and sometimes heatwave (Lu et al., 2018; Luo et al., 2017a). Compared with weather and climate isolated events, compound events can have severe socio-economic effects, even if the individual events that make up the compound event are not all extreme events (Ridder et al., 2020; Chapman et al., 2019). The occurrence and effects of CDH events have been studied extensively, increased frequency and severity of CDH events were reported across China (Kong et al., 2020; Luo et al., 2022), India (Sharma and Mujumdar, 2017), the United States (Mazdiyasni and AghaKouchak, 2015), and Europe (Manning et al., 2019). Further studies include the application of combined distribution and magnitude index to grade assessment (Wang et al., 2018; Zhang et al.,2022). Previous studies are generally based on stationarity hypothesis to calculate drought index. However, in the context of frequent

* Corresponding authors.
E-mail addresses: sun68peng@ahnu.edu.cn (P. Sun), zhangq68@bnu.edu.cn (Q. Zhang).

https://doi.org/10.1016/j.jhydrol.2022.128154
Received 12 December 2021; Received in revised form 23 June 2022; Accepted 1 July 2022
Available online 8 July 2022

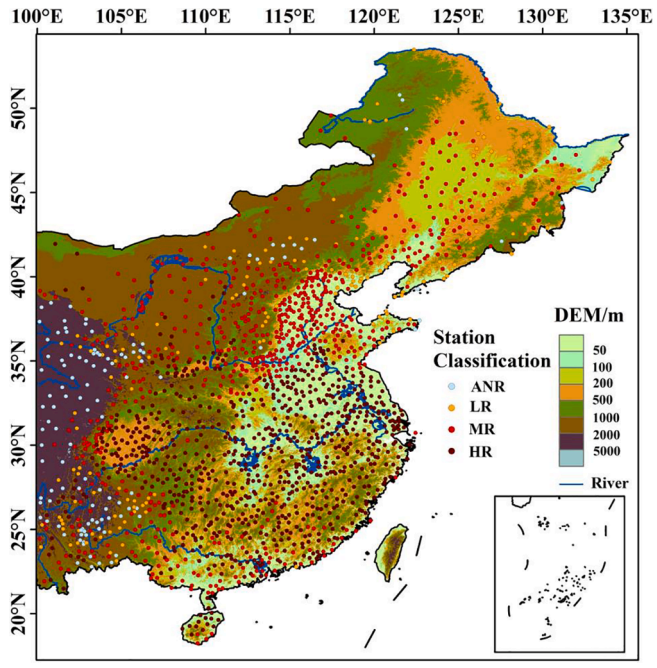

Fig. 1. Study area and the distribution of stations in eastern China.

human activities and global warming, stationary hypothesis has been gradually questioned (Gu et al., 2019; Rashid and Beecham, 2019). Recent studies in different parts of the world have showed that stationarity assumption has been difficult to apply to change of climate (Song et al., 2020; Zhang et al., 2021a). Therefore, it is necessary to study drought index based on non-stationary hypothesis. Moreover, it seems that drought promotes heat waves (Shi, et al., 2021). The temporal and spatial differences of such promoting effect still need further research, so as to explore the mechanism behind drought triggering and amplifying the heat waves, and provide a basis for possible further research in the future.

Eastern China (east of 100° E) is mainly characterized by a monsoon climate and the western North Pacific subtropical high (WNPSH), and it is also heavily populated and highly economically developed (Liu et al., 2019; Zheng et al., 2019). Located in the east part of Eurasia continent Eastern and neighbored to the Pacific Ocean, eastern China hence is highly sensitive to climate changes and weather extremes there have aroused considered concerns from academic community (Zhang et al., 2017; Chen and Zhai, 2017). However, the spatiotemporal behaviors of CHD in eastern China remain unclear and warrant further examinations. By using both relative and absolute air temperature thresholds to identify heatwaves, and using the non-stationary standardized precipitation evapotranspiration index (NSPEI) to identify drought events, here we analyzed spatiotemporal patterns of CDH across eastern China from 1970 to 2019 and quantified the relations of heatwaves with droughts and the changes of CDH events.

2. Data and methods

2.1. Data

The meteorological data during 1970–2019 used in this study were sourced from the National Climate Center of the China Meteorological Administration (CMA, https://data.cma.cn/). Specific variables include precipitation and temperature, wind speed, barometric pressure, sunshine hours, relative humidity, and other variables needed in the calculation of potential evapotranspiration. Considering the length of the data and excluding the stations with > 1% missing record, we selected 1784 meteorological stations covering most of eastern China (Fig. 1). And the meteorological stations were classified into four groups with different grades of duration and intensity of the heatwaves by hierarchical clustering method: stations with almost no risk of heatwaves (ANR), stations with low risk of heatwaves (LR), stations with medium risk of heatwaves (MR), and stations with high risk of heatwaves (HR). The missing data were processed based on cubic convolution. (Zhang, et al., 2011). And the WPSH intensity index was obtained from the Climate Monitoring Center of CMA. The geopotential height and other reanalysis data were obtained from theERA5 reanalysis datasets with 0.25 spatial resolution and month time resolution. (https://www.ecmwf.int/).

2.2. Methods

2.2.1. Definition of heatwaves

Heatwave event has been defined by CMA as a period with daily maximum temperature of ≥ 35 °C for at least 3 consecutive days (e.g., Shen et al., 2018). However, the heatwave indicators by absolute thresholds tend to underestimate the damage or losses caused by heatwaves at high latitudes and are not appropriate for analysis of heatwaves in various regions (Xie et al., 2020; Luo and Lau, 2021). The relative threshold by percentile of temperature can reflect the adaptation of inhabitants to high air temperature in different climate regimes. However, it is difficult to differentiate the high temperature based on the index and the actual high temperature (Ye et al., 2013). In this case, we took the relative and absolute temperature thresholds to define heatwaves. When T_{90} (i.e., 90th quantile temperature of the maximum daily summer temperature) ≥ 30 °C, $T_0 = T_{90}$; otherwise, when $T_{90} < 30$ °C, $T_0 = 30$ °C. A heatwave process occurs if the daily maximum temperature, i.e., $T_{max} \geq T_0$, lasts for ≥ 3 days. For the sake of spatiotemporal analysis of the heatwaves, we analyzed the heat wave frequency (HWF, the yearly number of heat waves), heat wave duration (HWD, the duration of a heatwave event), and heat wave intensity (HWI, the sum of the daily maximum temperatures during throughout a heatwave event) (Luo et al., 2020; Ye et al., 2013).

2.2.2. Non-stationary standardized precipitation evapotranspiration index

The standardized precipitation evapotranspiration index (SPEI) has been widely used in studies of meteorological drought (Beguería et al., 2014; Vicente-Serrano et al., 2010). However, SPEI assumes stationarity of the meteorological processes and may potentially overestimate the responses of meteorological droughts to warming climate. Here we proposed a non-stationary standardized precipitation evapotranspiration index (NSPEI) to monitor meteorological droughts across eastern China (Wen et al., 2020). It is to use time-varying position parameters to fit log-logistic distributions, the NSPEI was computed as follows:

(1) Calculate the difference, D_t, between monthly precipitation, P_t, and monthly PET_t:

$$D_t = P_t - PET_t \tag{1}$$

The smooth spline function was then used to fit D_t:

$$SS_{Dt}(h) = \sum_{t=1}^{n} [D_t - f(D_t)]^2 + h \int_{Dt_{min}}^{Dt_{max}} [f'(D_t)]^2 D_t \tag{2}$$

where f is a linear fitting function of D_t, h is a smoothing parameter, t is the time series, t = 1, …, n, and PET_t is the potential evapotranspiration based on the Penman-Monteith evapotranspiration formula. So, SS_{Dt} is a data series calculated by local polynomial regression fitting of D_t. According to Eq. (1) and Eq. (2), the time-varying position parameters, γ_{D_t}, can be obtained as follows:

$$\gamma_{D_t} = t(SS_{Dt})$$

In Eq. (3), the position parameter, γ_{D_t} is equal to SS_{Dt} at time t.

Table 1
Classification table for the NSPEI index corresponding to the drought grade.

Drought grade	NSPEI index
Mild drought	–0.99 < NSPEI ≤ 0
Moderate drought	–1.49 < NSPEI ≤ –1
Severe drought	–1.99 < NSPEI ≤ –1.5
Extreme drought	NSPEI < –2.0

(2) Calculate the log-logistic probability distribution, D_t:

$$f(D_t|\alpha,\beta,\gamma_{D_t}) = \frac{a}{\beta}\left(\frac{D_t-\gamma_{D_t}}{\alpha}\right)^{\beta-1}\left[1+\left(\frac{D_t-\gamma_{D_t}}{\alpha}\right)^{\beta}\right]^{-2} \quad (4)$$

$$F(x) = \int_0^x f(D_t|\alpha,\beta,\gamma_{D_t})dt\left[1+\left(\frac{\alpha}{D_t-\gamma_{D_t}}\right)^{\beta}\right]^{-1} \quad (5)$$

where α, β, and γ_{D_t} are the scale, shape, and position parameters, respectively.

(3) Estimate the parameters using probability weighting methods (PWMs) (Vicente-Serrano et al., 2010) based on the empirical frequency to compute NSPEI:

$$w_s = \frac{1}{N}\sum_{i=1}^{N}(1-F_i)^s D_i, F_i = \frac{i-0.35}{N} \quad (6)$$

$$NSPEI = W - \frac{C_0+C_2+C_3w_s^2}{1+d_1w_s+d_2w_s^2+d_3w_s^3}, W = \sqrt{-2\ln(P)} \quad (7)$$

In Eq. (6), N is the number of data series, and F_i is the frequency estimation, Ws is the s order of PWM. In Eq. (7), when $P \le 0.5$, P is the cumulative probability and $P = 1 - F(x)$; when $P > 0.5$, $P = 1 - P$. The other parameters are as follows: $C_0 = 2.515517$, $C_1 = 0.802853$, $C_2 = 0.010328$, $d_1 = 1.432788$, $d_2 = 0.189269$, and $d_3 = 0.001308$. Table 1 presents the classification table for the NSPEI.

2.2.3. CDH events and compound event magnitude index

A CDH event refers to the synchronous occurrence of meteorological drought and heatwave. We identified the monthly drought conditions based on the NSPEI index: heatwave events that occur in dry months (according to the starting date of the heatwave process) are considered as CDH events (Kong et al., 2020). The CDH frequency was calculated based on the dry months in which the heatwave occurred (no matter how many heatwaves occurred in that month). Besides, we also analyzed the occurrence probability of heatwave events in a backdrop of atmospheric drying conditions, where the number of dry months with heatwave events (regardless of the number of heatwave processes) were subdivided by the total number of dry months. We have analyzed the annual frequency of CDH events (CDHF, months with CDH events per year) and the variations in the compound drought heatwave magnitude index (CDHMI). And the maximum duration of CDH events reflects the maximum duration of heatwave days in a drought context. The CDHMI is calculated based on the probability of heat wave and drought events exceeding normal thresholds and reflects the intensity of the composite event to some extent (Wang et al., 2021; Wu et al, 2019; Zhang et al., 2021c). The CDHMI is calculated as follows (Fig. 2):

$$\text{CDHMI} = P_D(|\Delta D|)P_T\left(\sum_{i=1}^{n}\Delta T_n\right)$$

ΔD indicated the magnitude of drought, which is the difference between monthly drought indicator NSPEI and the drought threshold (the threshold was 0 according to the NSPEI calculation), and ΔD = 0 if no drought occurs in the month. ΔT indicated the magnitude of heatwaves, which is the difference between the maximum temperature and the temperature threshold T_0 during all heatwave occurrences, and the temperature threshold was determined in a similar way to 2.2.2. And n is the number of days in the month on which the CDH event occurred (number of all heatwave days in the month). $P_D(|\Delta D|)$ and $P_T(\Delta T)$ are the probabilities of ΔD and ΔT obtained from empirical distributions based on non-parametric distributions.

2.2.4. Statistical methods

Here, we used correlations by the Kendall τ test (Ribeiro et al., 2020) to analyze the spatiotemporal distributions of heatwave events. The generalized Pareto (GP) distribution was used to fit the duration and intensity of composite heatwave events (Huang et al, 2021). We calculated the spatiotemporal variation in the return periods and the probability density distributions of the heatwave duration and intensity for each station. Kernel density estimation is a non-parametric test method that can examine the distribution characteristics of data from the data itself (Okabe et al., 2009), and it was used to analyze the characteristics of the probability of heatwaves under a dry condition at monthly scale.

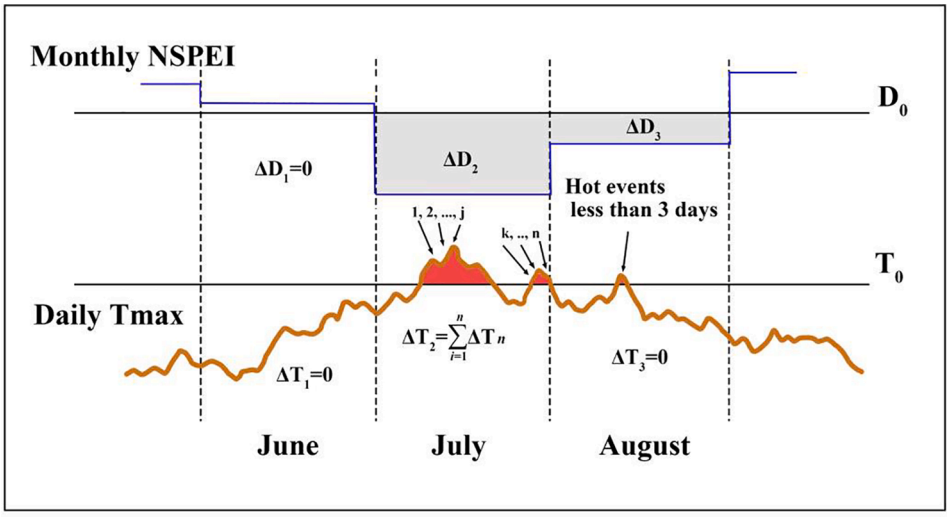

Fig. 2. CDHMI illustration based on drought indicator (NSPEI, Threshold D_0) and daily maximum temperature (Tmax, Threshold T_0). The blue line is NSPEI series, and the red curve is the daily Tmax series. When $\Delta D > D_0$, $\Delta D = 0$. When $\Delta T < T_0$, $\Delta T = 0$. ΔT is the difference between Tmax and T_0 for all days during the occurrence of a CDH event.

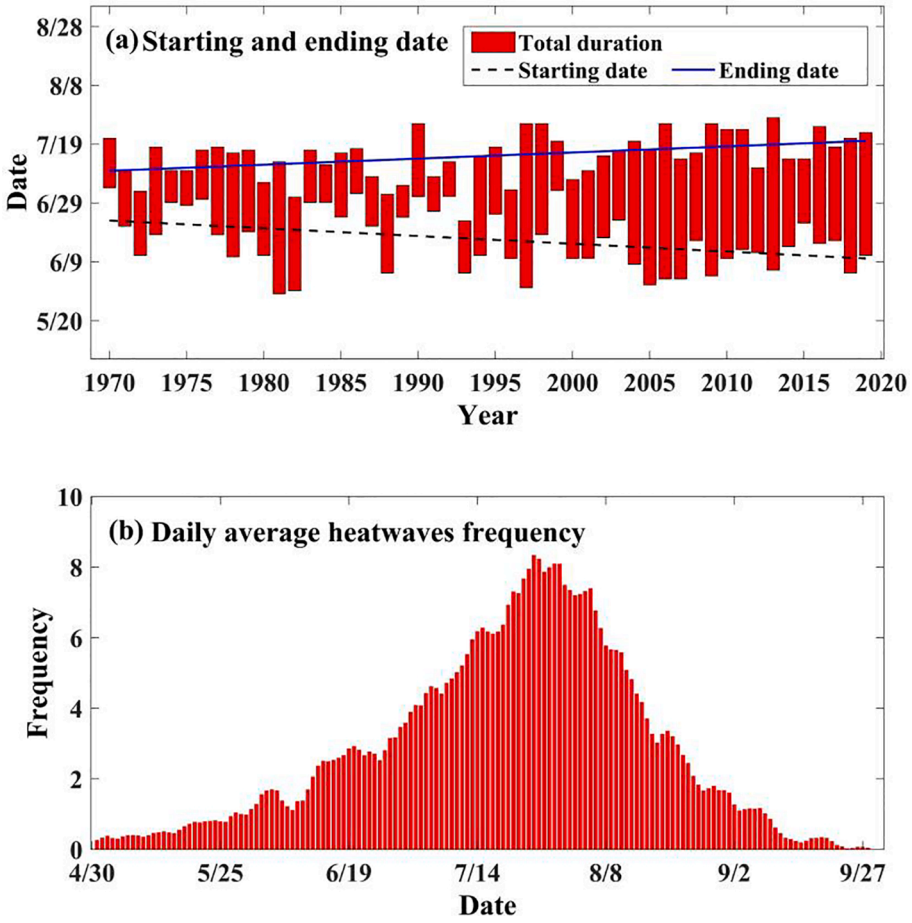

Fig. 3. (a) Changes in starting, ending date and total duration of heatwaves; (b) Distribution of daily average frequency of heatwaves within a year.

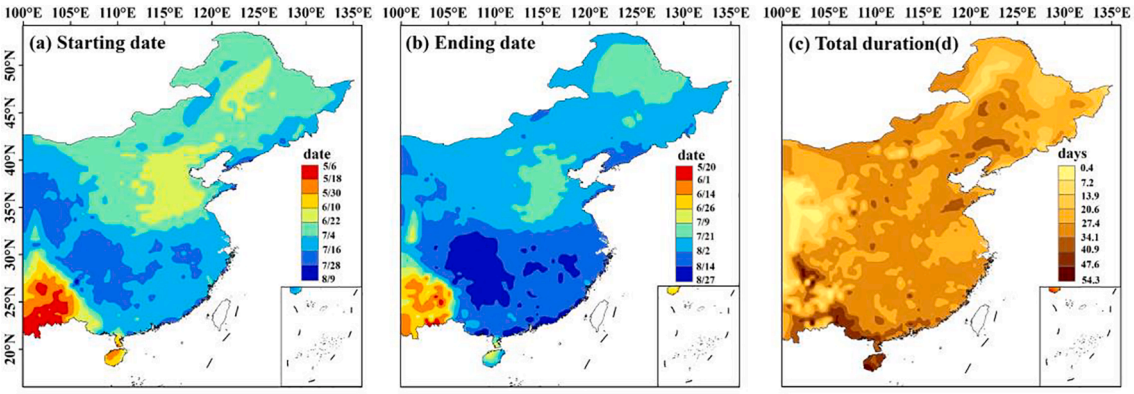

Fig. 4. Spatial distribution of the (a) starting date, (b) ending date, and (c) total heatwave duration of heatwaves across eastern China.

3. Results

3.1. Spatiotemporal patterns of heatwaves

We counted the median start date/ending date of the first/last heatwave events for each year at all stations over eastern China. We found that the start date of the heatwaves tended to be earlier while the ending date tended to be prolonged (Fig. 3a), implying lengthening heatwave events over the past decades. We calculated the average frequency of daily heatwaves (total number of heatwaves occurring at all stations during 1970–2019 divided by the total number of stations) (Fig. 3b), heatwave events occurred mainly in late July and early August; the frequency of daily heatwaves gradually increased from May and fewer heatwaves can be detected in September.

According to the spatial distribution of the onset date of the first heatwaves, the ending date of the last heatwaves, and the average total heatwave duration within a year (Fig. 4), the first heatwave event occurred in May from Yunnan-Guizhou Plateau to Hainan Island, with a relatively long duration (Fig. 4c). The first heatwave in large regions of southern China began in mid-July and usually ended in late August. In the North China Plain, the first heatwave event started earlier in June but the total duration was shorter, and the last heatwave ended in late July. The onset of heatwaves in northern China was earlier than that in most parts of southern China; the end of the last heatwave in southern

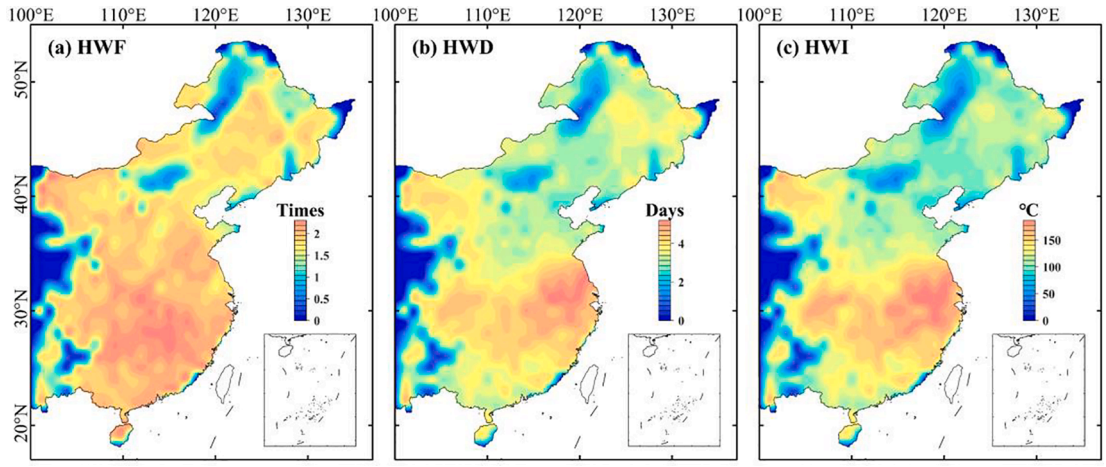

Fig. 5. Spatial distribution of climatological mean heatwave metrics in eastern China: (a) heat wave frequency (HWF), (b) heat wave intensity (HWI), and (c) heat wave duration (HWD).

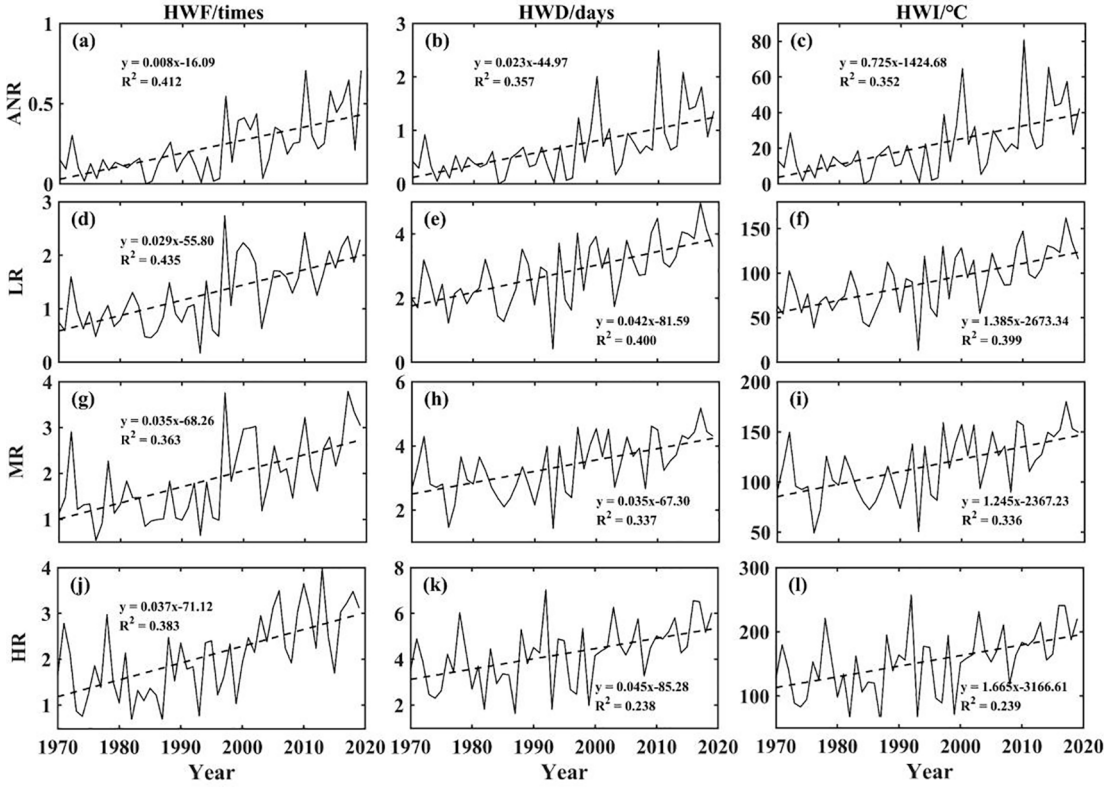

Fig. 6. Yearly time series of HWF, HWD, and HWI for different groups of stations: Almost no risk, low risk, medium risk, high risk.

China was significantly later than that in northern China. In the Yunnan-Guizhou Plateau, the onset of heatwaves was the earliest with the longest total duration.

Fig. 5 shows the distribution of each heatwave indicator. In most of the eastern region. There are no large differences in HWF, and heatwaves occur slightly more frequently in the south than in the north. Heatwaves affected most parts of eastern China every year, except for central Inner Mongolia, and northern Heilongjiang region. The HWF and the HWD of a single heatwave event were highly consistent in their spatial distributions; the high values of HWI and HWD were concentrated in the plains along the middle and lower Yangtze River basin, Sichuan Basin, and the western Inner Mongolia. The mean HWI was approximately 200 °C. Long-duration heatwaves (generally lasting for approximately 4–6 days) were more concentrated along the coastal regions of eastern China. Although the HWF in northern and northeastern China was not distinctly different from that in the Yangtze-Huai River Basin, the intensity and duration of the heatwaves were evidently lower than those in the Yangtze-Huai River Basin (Fig. 5b, c).

After 2000, the annual frequency and intensity of heatwaves were evidently higher than those prior to 2000 for stations in ANRs, LRs, and HRs, as identified in heatwave indicators (Fig. 6). The variation in the HWD was not evident for most regions of the study area; the HWD was shorter at the stations with less heat waves. The average frequency of heatwaves from 1970 to 1980 was 1.39, and it increased to 1.93 in 1981–2019. After 1980, all heatwave metrics exhibited significant upward trends at significance level.

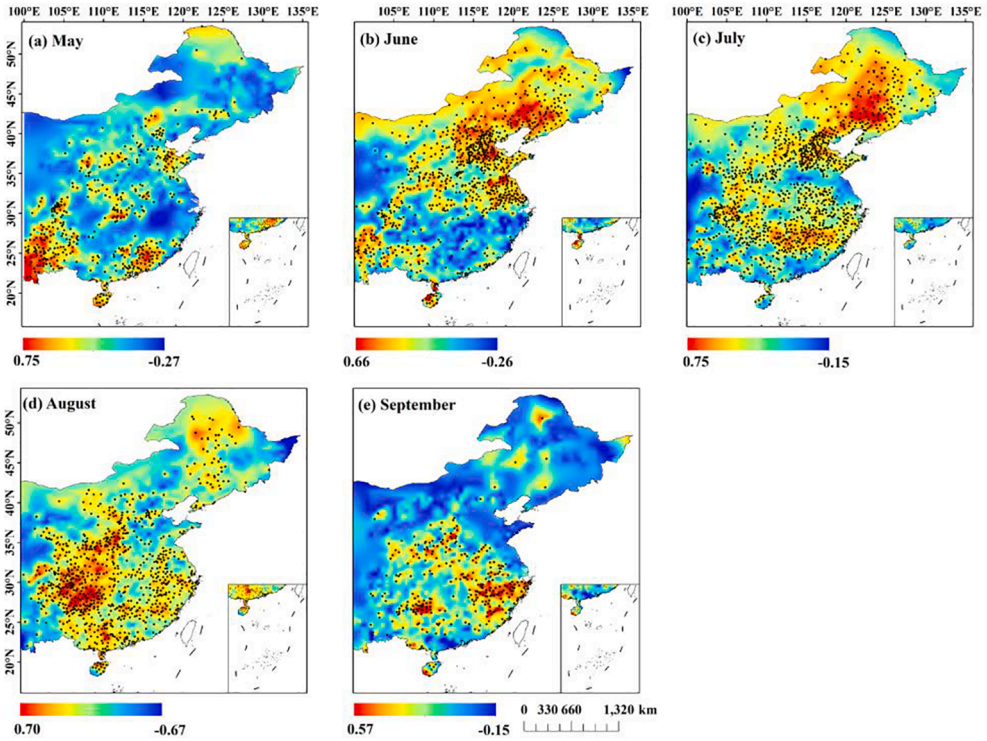

Fig. 7. Spatial distribution of correlation coefficients of the drought intensity with the heatwave duration in different months from May to September.

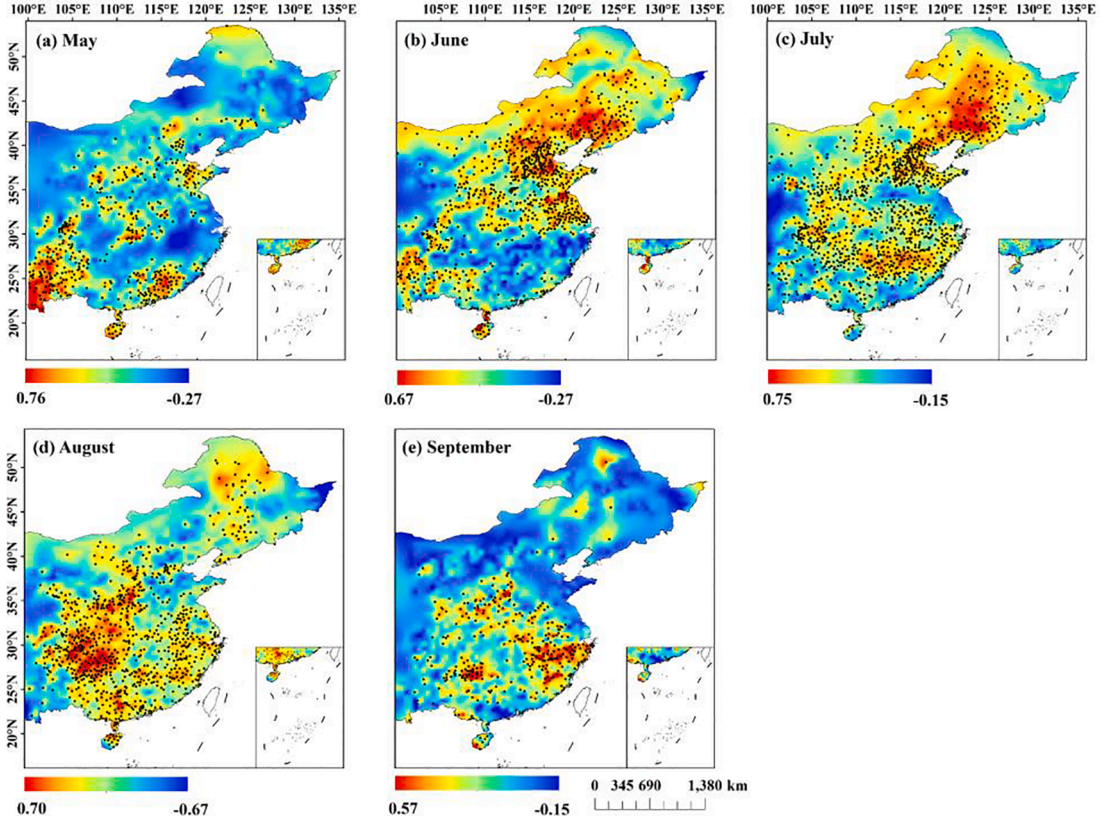

Fig. 8. As Fig. 7 but for the heatwave intensity (HWI).

3.2. Correlation between heatwaves and meteorological droughts

Here, we quantified the correlation coefficients between drought intensity and heatwave duration and intensity at stations with different heatwave grades in various months given the occurrence of droughts with NSPEI ≤ 0. Generally, the correlation coefficients between drought

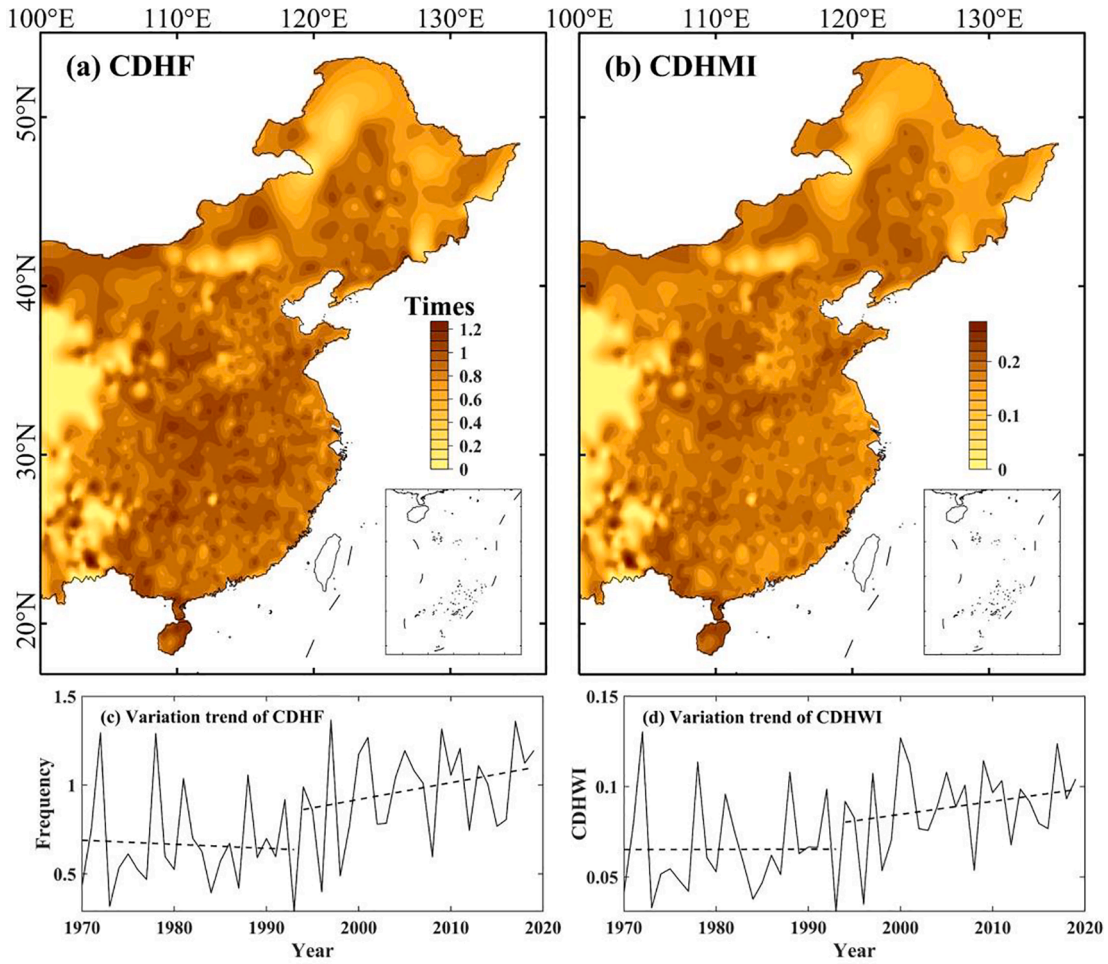

Fig. 9. Spatiotemporal changes in CDHF and CDHWI: (a) CDHF changes in space and (c) trends; (b) CDHWI changes in space and (d) trends.

intensity and heatwave duration and intensity are regionally varying. Figs. 7 and 8 collectively illustrate the spatial distribution of correlation coefficients between drought intensity and HWD and intensity for each month. The stations marked in Figs. 7 and 8 are characterized by significant correlations between drought intensity and HWD and intensity at 0.05 significance level. And the negative correlations between drought intensity and the duration and intensity of heatwaves rarely passing the significance test. In May and September, no significant correlations between drought and heatwave were detected in most parts of eastern China; significant correlations between drought and heatwave were detected mainly in the Yunnan–Guizhou Plateau in May and in some areas of southern China in September. In July, positive correlations between heatwave and drought were found in the Northeast China Plain, but correlations between drought and heatwave were not significant in eastern parts of Northeast China Plain. High correlations between drought and heatwave from July to September were found mainly in northeast China and the Yangtze-Huai River Basin. Droughts from July to September exhibited significant correlations with heatwave duration and intensity in northeast China and the Yangtze–Huai River Basin.

3.3. Spatiotemporal characteristics of CDH

It can be seen in Fig. 9 that high CDHF was found mainly across the Northeast China Plain to the middle and lower Yangtze River Basin. Most regions of eastern China were characterized by one CDH per year (Fig. 9a). Besides, the CDHF was also of 0.12/10a in increasing magnitude; meanwhile, an upward trend of 0.2/10a in CDH was also detected from 1990 to 2019. After 2000, CDH events were subject to persistent a high frequency (Fig. 9c). The CDHMI and CDHF shows the same spatial distribution, and is more concentrated in the northern part of China. In particular, the rising trend of CDNI became significant after 2000 (Fig. 9b, 9d).

Fig. 10 shows the spatial distribution of the maximum duration and CDHMI of the CDH event for the 20-, 50- and 100-year recurrence period. The spatial distribution of maximum duration and CDHMI is basically the same. However, CDHMI is more concentrated in the area north of the Huaihe River, where high values of maximum duration reaching around 15, 20 and 23 days for the 20-, 50- and 100-year events, and high values of CDHMI above 0.3, 0.4 and 0.5 respectively. Most areas in eastern China have a high risk of heat waves, CDH events can cause greater loss and harm as the recurrence period increases.

3.4. Effects of drought on heatwaves

We now proceed to evaluate the probability of heatwave events under the occurrence of droughts. The peak value of the kernel density estimation can reflect the central tendency in the sample dataset. As indicated in Fig. 11, the peak probabilities of heatwave with drought in May and September were approximately 0, was 0.14 and 0.59 in June, 0.67 in July, and 0.53 in August. The probability of heatwaves under the occurrence of droughts in May and September was low. While heatwaves and drought are frequent from June to August, such that CDH events were frequent. Fig. 11a shows the spatial distribution of the heatwave probabilities under droughts from May to September. In May, higher probability can be mainly identified in the Yunnan-Guizhou

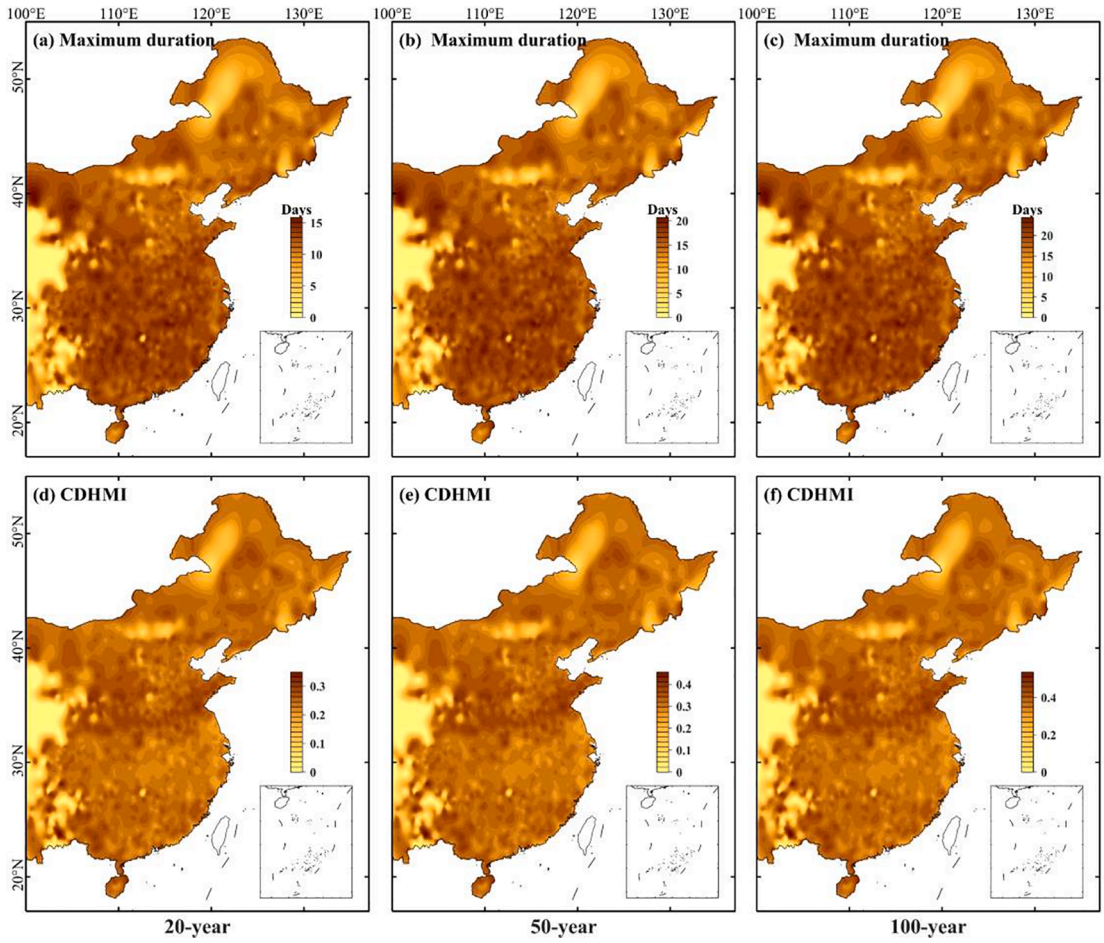

Fig. 10. Spatial distribution of the Maximum duration (upper panel) and magnitude index (CDHMI; bottom panel) of the CDH events with return periods of 20 (left), 50 (center), and 100 (right) years.

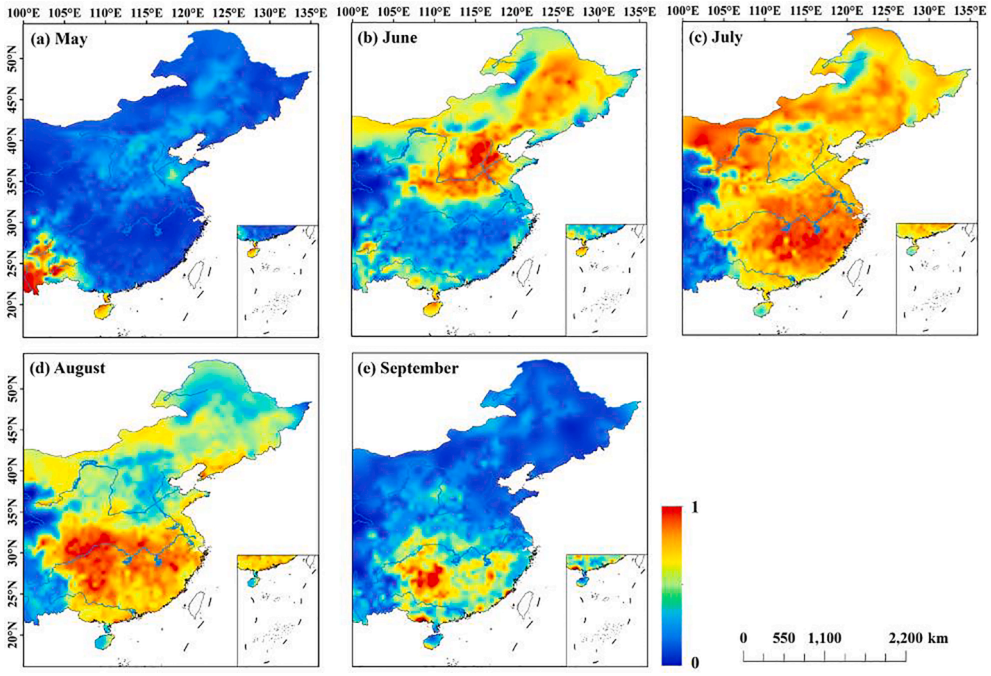

Fig. 11. Spatial distributions of the probability of heatwaves under the occurrence of droughts in different months from May to September.

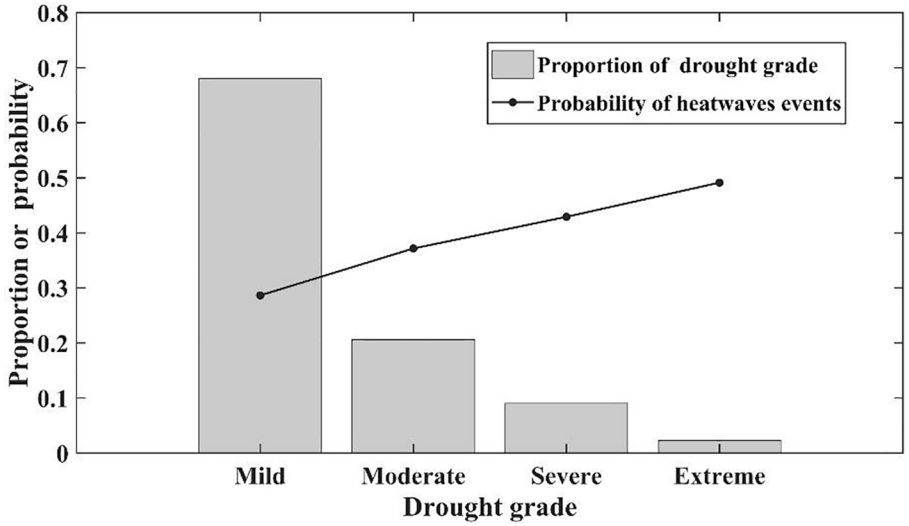

Fig. 12. Probability of heatwaves under different drought conditions.

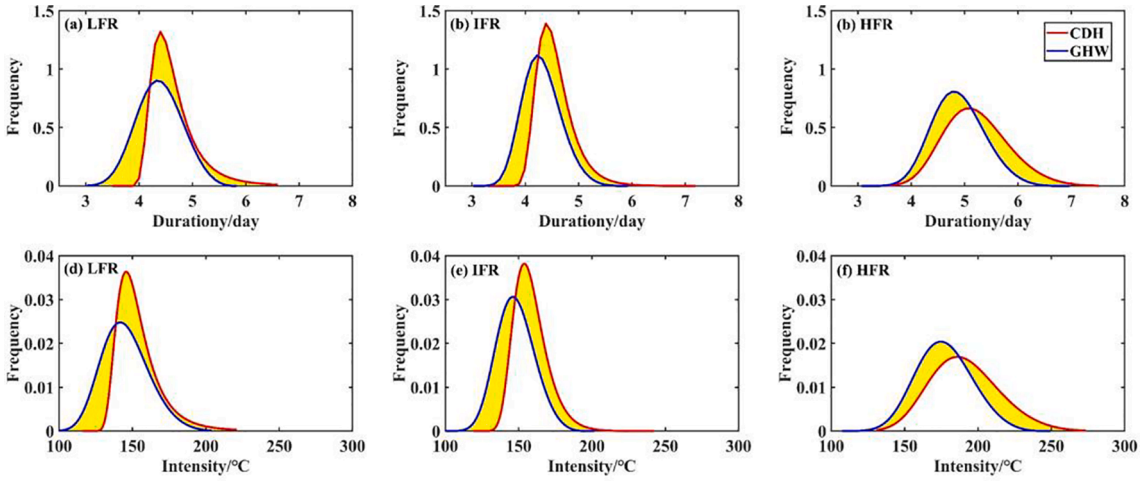

Fig. 13. Probability densities for the duration (upper panel) and intensity (bottom panel) of CDH and GHW events in different clustered subregions of eastern China.

Plateau and low probability (approximately 0) appears in most parts of eastern China. In June, higher probability can be identified in most areas of the North China Plain and the Loess Plateau and low probability is mainly seen in the Yangtze-Huai River Basin. In July, the center with higher probability of heatwaves with drought shifted to the Yangtze-Huai River Basin and the Inner Mongolia Plateau. In most portions of eastern China, drought events were highly likely to trigger heatwaves. In August, higher probability are seen in the southern Yangtze-Huai River Basin; the probability in most regions of eastern China was higher than 0.5. In September, the range of high probabilities was small and high probability can be found only kin the Pearl River basin and the Ganjiang River basin.

It can also be seen in Fig. 11 that the impacts of droughts on heatwaves vary across both space and time. Droughts in July were sensitive to heatwaves in most parts of eastern China. Based on Fig. 3b,and 11, there were few heatwaves in September, and the heatwave duration and intensity were significantly correlated with droughts. Therefore, the heatwave process in southern China in September was closely related to drought.

Fig. 12 shows the proportions of droughts with different intensities and the probability of heatwaves under different drought conditions (i.e., with different intensities). Although the proportion of extreme drought (0.02) was significantly lower than that of mild drought (0.68), the probability of a heatwave given extreme drought was the highest, reaching 0.49. The higher the drought level, the lower the occurrence proportion of droughts, but the higher the probability of heatwaves, implying that higher drought intensity can potentially trigger occurrence of heatwaves.

Drought has a significant influence on heatwave duration and intensity. Fig. 13 shows the probability densities for the duration and intensity of CDH and GHW (see Methods) events in different clustered subregions of eastern China. The duration and intensity of the CDH events under the influence of drought generally shifted to the right side, where the peak value position of the probability density curve was higher than that of the GHW events. This indicates that the intensity of CDH events was larger, the duration was longer, and these events tend to cause more serious damage.

The CDH duration (intensity) was 0.27 (8.84 ℃), 0.25 (10.37 ℃), and 0.34 d (14.20 ℃) longer than that of GHW events in the regions of low-, medium-, and high-risk of heatwaves, respectively. The differences in the duration and intensity of the CDH and GHW events are compared in Fig. 14. In most parts of eastern China, the duration and intensity of the CDH events were greater than those of heatwaves with lower intensity and shorter duration. This evident difference was found across the Yunnan-Guizhou Plateau, Qinghai-Tibet Plateau, and northeast China, where the heatwave frequency was low. The difference in the

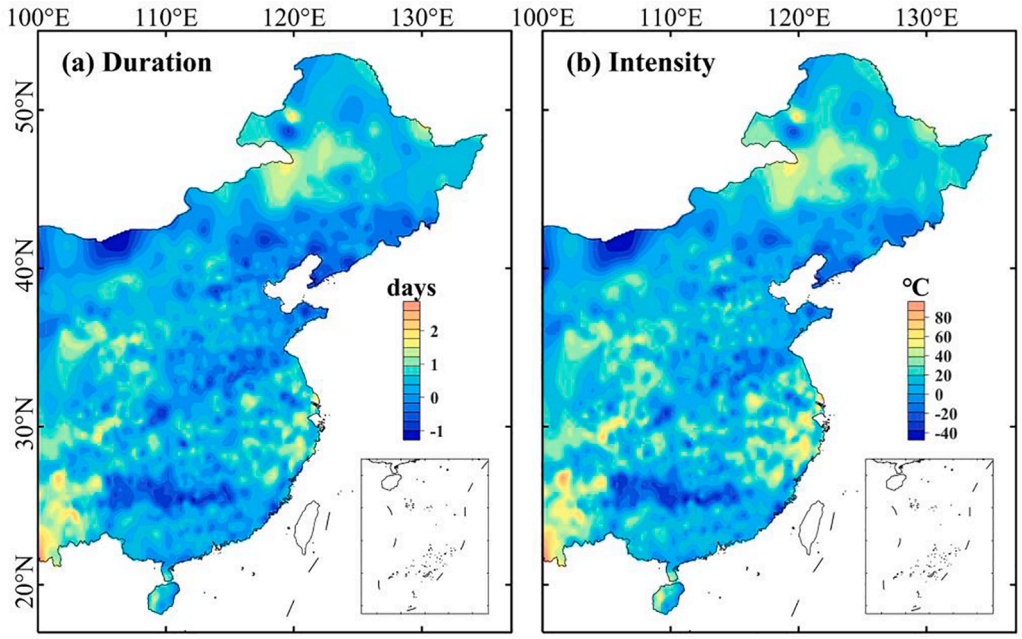

Fig. 14. Spatial distribution of the difference in the average (a) duration and (b) intensity between CDH and GHW events (i.e., CDH minus GHW).

largest duration (intensity) was up to 3.0 d (95.2 ℃) between the CDH and GHW events, but a negative average difference is shown in the southern region, such as Guangdong and Guangxi provinces with frequent heatwaves. The duration (intensity) of heatwaves is longer (stronger) under a drought background in areas with few heatwaves, implying that the effects of drought on heatwave is more significant in areas with less frequent heatwave.

4. Discussions

Indices based on different temperature thresholds often have certain uncertainties in definition of heatwave regimes, which may be due to differences in the spatial and temporal distribution of various temperature thresholds (You et al., 2016). Absolute temperature thresholds have been often used in studies at regional scales, whereas relative thresholds have been widely used in studies at larger temporal or spatial scales (Luo et al., 2020; Trancoso et al 2020). Eastern China is a vast territory with significant climate differences, where the inhabitants of different subregions show different adaptations to high temperatures. Therefore, selecting a unified index to measure changes in heatwaves across all of eastern China is complex. In this study, a combination of relative and absolute thresholds was selected to identify heatwaves to avoid the occurrence of an excessively low threshold in high-latitude and high-altitude areas when applying a relative threshold to analyze heatwaves across the entire study area, demonstrating a certain rationality and applicability (Wu et al., 2020; Ye et al., 2013). Studies based on different thresholds have reported the increases in the heatwave frequency, duration, and intensity at regional and global scales (Kong et al., 2020; Manning et al., 2019; Mazdiyasni and AghaKouchak, 2015), which is similar to the observations obtained in this study. In eastern China, the upward trend in the heatwave frequency, duration, and intensity was more significant since 2000.

There is a connection between heatwave events and global climate change. Although studies have shown that there is a current slowing of global warming, extreme high temperature events occur with higher frequency in China (Li et al., 2021b; Wang et al., 2016). Additionally,

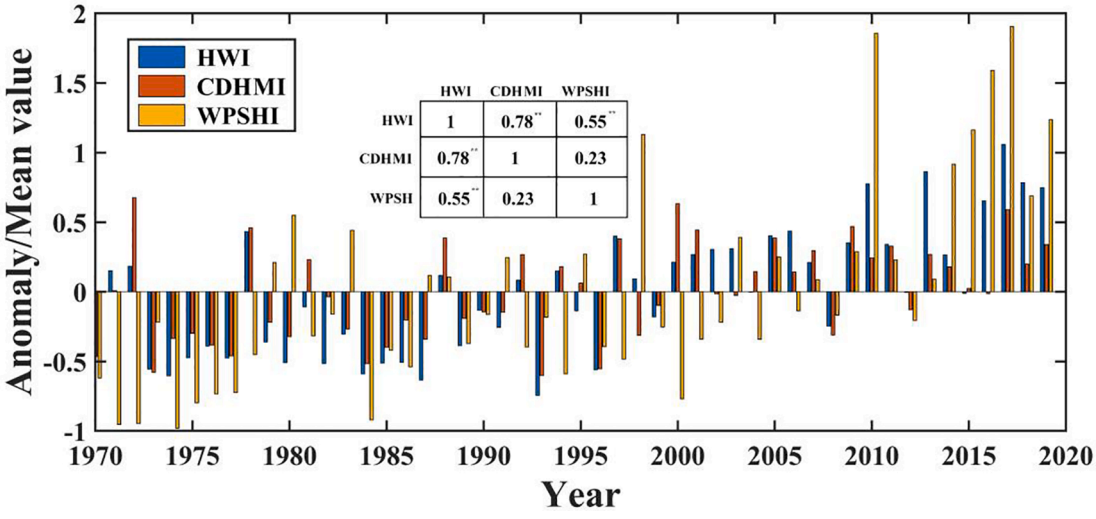

Fig. 15. Variations of the anomalies of heatwave intensity in Eastern China and the western Pacific subtropical high (WPSH) intensity index from 1970 to 2017.

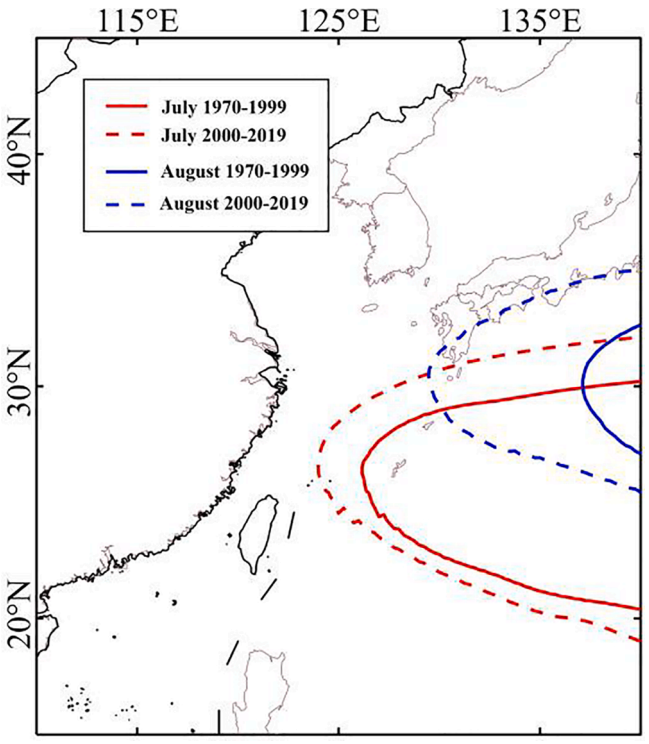

Fig. 16. Average contour map of the 500 hPa geopotential height field in July and August ca. 2000. The red and blue line denotes the 5880 m characteristic line of the WPSH.

many studies have discussed the causes behind heatwaves in China from an atmospheric circulation perspective. The El Niño phenomenon strengthens the anticyclone and subtropical high in the western Pacific, thus providing favorable conditions for the occurrence and maintenance of heatwaves (Luo and Lau, 2018) also pointed out that heatwave activity increases in the summer after the El Niño phenomenon. Moreover, the WPSH exerts significant impacts on heatwaves in eastern China, with a wide range of air subsidence, frequent high temperatures, and negligible precipitation in the control area of the WPSH ridge (Liu et al., 2019; Ma et al., 2020). Fig. 15 shows the interannual variation in HWI, CDHMI and WPSH intensity index (WPSHI) in May-September. In most years, the HWI and WPSHI change synergistically, and their correlation coefficient between the heatwave intensity and WPSH intensity reached 0.55, passing the 0.05 significance test. In contrast, the direct correlation between CDHMI and WPSHI was not significant, but the correlation between HWI and CDHMI showed a high correlation (passing the 0.05 significance test). It can be seen that to some extent the WPSH have a greater influence on the general heat wave than CDH event.

Fig. 16 shows the change in the 500 hPa geopotential height field in July and August, i.e., the hottest summer months, before and after 2000 (mutation year). The average position of the WPSH after 2000 was more westward than that before 2000. The changes in the intensity and position of the WPSH should be one of the reasons for the frequent heatwave occurrence in eastern China after 2000. It is noted that the abnormal westward movement of the WPSH resulted in an abnormally high pressure and high temperature evolution, such that heatwaves in southern China were often accompanied by an abnormal high-pressure center and near-surface anticyclonic while simultaneously reducing the water vapor transport between the land and sea (Luo and Lau, 2017b).

CDH events in eastern China have been widely discussed. Some scholars have established the standardized compound drought and heat index (SCDHI)for the evaluation of CDH events in China, they found the occurrence frequency of CDH events is high in South China (Li et al., 2021a). The dry-hot magnitude index also has a wide range of applications in the analysis of composite events (Wang et al., 2021; Wu et al., 2019). The researchers found that high magnitude levels of composite dry-hot events occurred mainly in northeast and southwest China, and mainly in recent decades since the 1990 s. Based on the NSPEI index, we analyzed the frequency and trend of CDH events based on the identification of concurrent drought and heatwave events, and found that CDH events generally occurred in the Northeast Plain, North China Plain, and Yangtze-Huai River Basin. There is a connection between compound events and large-scale climate change (Mukherjee and Mishra, 2020), based on Poisson generalized linear model, the occurrence of compound

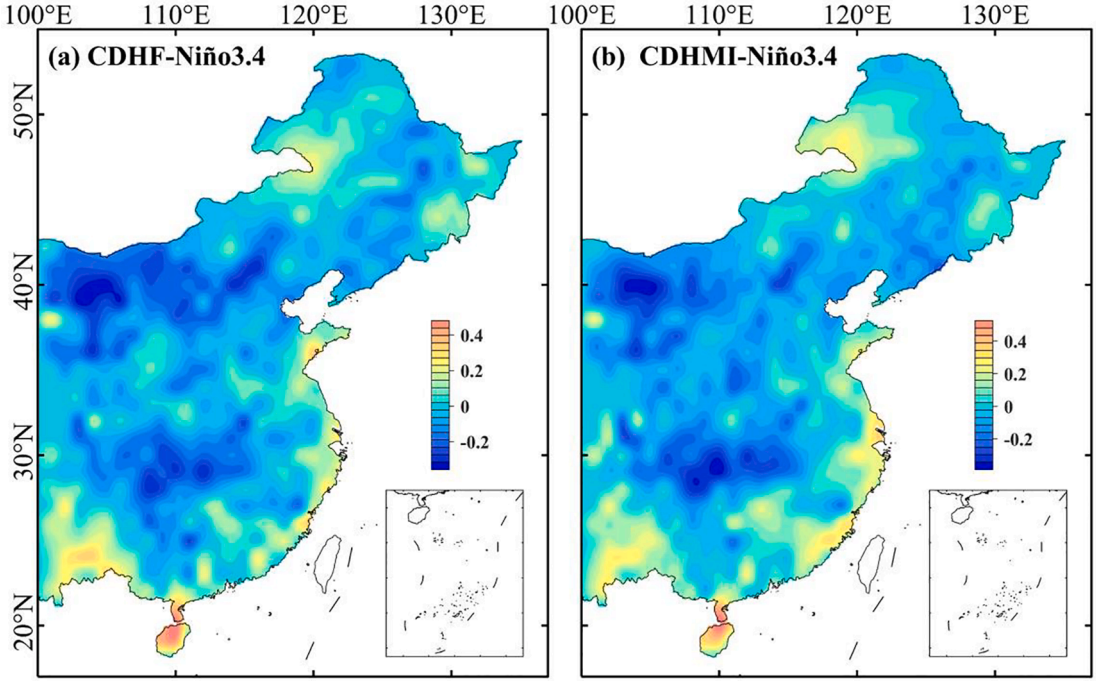

Fig.17. Correlation coefficients between CDHF(a) and CDHMI(b) and Niño3.4.

events and El Nino Southern Oscillation (ENSO) show a strong correlation in the southern hemisphere. Then, we further analyzed the degree of correlation between ENSO (East Central Tropical Pacific Temperature) and CDHMI and made the following spatial distribution of correlation (Fig. 17). Considering that the development of Niño 3.4 is most obvious in winter (Zambrano Mera et al., 2018), we performed a correlation analysis using Niño 3.4 values of previous winter. It can be seen that the correlation coefficients of Niño 34 and CDHF, CDHMI are basically consistent in spatial distribution, showing mainly positive correlation in coastal areas, but negative correlation in most regions of the country, especially in Inner Mongolia and the middle and lower reaches of the Yangtze River.

The probability of concurrent heatwaves in different summer months under a drought background varied with space; heatwave events occurred less in most parts of eastern China in May. Owing to the influence of large-scale climate circulation, plum rain is annually concentrated in areas between the Yangtze River and Huai from early June to July (Zhou et al., 2021) and drought events rarely occur, which explains the low CDH event probability in the Yangtze-Huai River basin under a drought background in May and June. However, droughts in July and August are often accompanied by heatwaves, which pose human and ecological health threats. The response of droughts to heatwaves may be closely related to the water vapor transport and circulation background, which requires further investigations. Additionally, studies have found that urbanization and other anthropogenic influences have significantly increased the occurrence of extremely high temperatures in summer in China since the beginning of the 21st century (Wang et al., 2018; Zhang et al., 2021b), such that we cannot underestimate the influence that human factors have on heatwaves and droughts.

5. Conclusions

Based on daily meteorological data at 1,784 meteorological stations in eastern China from 1960 to 2019, this study analyzed the temporal and spatial distribution of various heatwave metrics, the frequency of CDH events, and their relationships with meteorological droughts in eastern China. The main conclusions are as follows.

(1) The heatwaves from May to September in eastern China tended to start earlier and end later, with a prolonging trend in the duration. The frequency, duration, and intensity of heatwaves, and the frequency of CDH events significantly increase after 2000. The heatwave events were mainly distributed from the plains along the middle and lower reaches of the Yangtze River to the Sichuan Basin; whereas the CDH events were mainly distributed from the northeastern plains to the middle and lower reaches of the Yangtze River.
(2) There was a significant correlation between the drought intensity and heatwave duration and intensity in northeastern China and the Yangtze–Huai River Basin from July to September; the effect that droughts had on the heatwave intensity was more significant. Under the influence of drought, the heatwave intensity was greater and the heatwave duration was longer; the promoting effect of drought was more significant in the northern and some southern regions where heatwave occurrence is less frequent.
(3) Heatwaves in eastern China were influenced by the WPSH; the heatwave intensity and WPSH intensity index tended to exhibit coordinated variation. After 2000, the mean position and intensity of the WPSH were west and strong, respectively, which were closely related to heatwave occurrences in eastern China.

CRediT authorship contribution statement

Yaojin Bian: Conceptualization, Methodology, Software. **Peng Sun:** Data curation, Writing – original draft, Visualization, Investigation. **Qiang Zhang:** Data curation, Writing – original draft. **Ming Luo:** Writing – review & editing. **Ruilin Liu:** Writing – review & editing.

Declaration of Competing Interest

The authors declare that they have no known competing financial interests or personal relationships that could have appeared to influence the work reported in this paper.

Data availability

The authors do not have permission to share data.

Acknowledgments

This research is partially funded by National Natural Science Foundation of China (42041006), National Key R&D Program of China (2019YFA0606900), Nature Science Foundation for Excellent Young Scholars of Anhui (2108085Y13), Key Research and Development Program Project of Anhui province, China (2022m07020011), Anhui Major Science and Technology Projects (202003a06020002), The University Synergy Innovation Program of Anhui Province (GXXT-2021-048), University Outstanding Young Talents Support Project of Anhui (gxyqZD2021094).

References

Beguería, S., Vicente-Serrano, S.M., Reig, F., Latorre, B., 2014. Standardized precipitation evapotranspiration index (SPEI) revisited: parameter fitting, evapotranspiration models, tools, datasets and drought monitoring. Int. J. Climatol. 34 (10), 3001–3023. https://doi.org/10.1002/joc.3887.

Bras, T.A., Julia, S., Nuno, C., Jagermeyr, J., 2021. Severity of drought and heatwave crop losses tripled over the last five decades in Europe. Environ. Res. Lett. 16 (6), 065012 https://doi.org/10.1088/1748-9326/ABF004.

Chapman, S.C., Watkins, N.W., Stainforth, D.A., 2019. Warming Trends in Summer Heatwaves. Geophys. Res. Lett. 46 (3), 1634–1640. https://doi.org/10.1029/2018GL081004.

Chen, Y., Zhai, P., 2017. Revisiting summertime hot extremes in China during 1961–2015: overlooked compound extremes and significant changes. Geophys. Res. Lett. 44 (10), 5096–5103. https://doi.org/10.1002/2016GL072281.

Gao, T., Zhang, Q., Luo, M., 2019. Intensifying effects of El Niño events on winter precipitation extremes in southeastern China. Clim. Dyn. 54, 631–648. https://doi.org/10.1007/s00382-019-05022-6.

Gu, X., Zhang, Q., Li, J., Singh, V.P., Sun, P., 2019. Impact of urbanization on long-term changes and nonstationarity of annual and seasonal precipitation extremes in China. J. Hydrol. 575, 638–655. https://doi.org/10.1016/j.jhydrol.2019.05.070.

Huang, H., Cui, H., Ge, Q., 2021. Assessment of potential risks induced by increasing extreme precipitation under climate change. Nat. Hazards 108 (2), 2059–2079. https://doi.org/10.1007/s11069-021-04768-9.

Kong, Q., Guerreiro, S.B., Blenkinsop, S., Li, X., Fowler, H.J., 2020. Increases in summertime concurrent drought and heatwave in Eastern China. Weather Clim. Extremes 28, 100242. https://doi.org/10.1016/j.wace.2019.100242.

Leonard, M., Westra, S., Phatak, A., Lambert, M., van den Hurk, B., McInnes, K., Risbey, J., Schuster, S., Jakob, D., Stafford-Smith, M., 2014. A compound event framework for understanding extreme impacts. Wiley Interdiscip. Rev. Clim. Change 5 (1), 113–128. https://doi.org/10.1002/WCC.252.

Li, X., Ren, G., Wang, S., You, Q., Sun, Y., Ma, Y., Wang, D., Zhang, W., 2021b. Change in the heatwave statistical characteristics over China during the climate warming slowdown. Atmos. Res. 247, 105152.

Li, J., Wang, Z., Wu, X., Zscheischler, J., Guo, S., Chen, X., 2021a. A standardized index for assessing sub-monthly compound dry and hot conditions with application in China. Hydrol. Earth Syst. Sci. 25 (3), 1587–1601. https://doi.org/10.5194/hess-25-1587-2021.

Liu, X., He, B., Guo, L., Huang, L., Chen, D., 2020. Similarities and Differences in the Mechanisms Causing the European Summer Heatwaves in 2003, 2010, and 2018. Earth's Future 8 (4). https://doi.org/10.1029/2019EF001386.

Liu, Q., Zhou, T., Mao, H., Fu, C., 2019. Decadal Variations in the Relationship between the Western Pacific Subtropical High and Summer Heat Waves in East China. J. Clim. 32 (5), 1627–1640. https://doi.org/10.1175/JCLI-D-18-0093.1.

Lu, Y., Hu, H., Li, C., Tian, F., 2018. Increasing compound events of extreme hot and dry days during growing seasons of wheat and maize in China. Sci. Rep. 8 (23), 2021–2035. https://doi.org/10.1038/s41598-018-34215-y.

Luo, L., Apps, D., Arcand, S., Xu, H., Pan, M., Hoerling, M., 2017a. Contribution of temperature and precipitation anomalies to the California drought during 2012–2015. Geophys. Res. Lett. 44 (7), 3184–3192. https://doi.org/10.1002/2016GL072027.

Luo, M., Lau, N., 2017b. Heat waves in southern China: Synoptic behavior, long-term change and urbanization effects. J. Clim. 30 (2), 703–720. https://doi.org/10.1175/JCLI-D-16-0269.1.
Luo, M., Lau, N., 2018. Amplifying effect of ENSO on heat waves in China. Clim. Dyn. 52 (5–6), 3277–3289. https://doi.org/10.1007/s00382-018-4322-0.
Luo, M., Lau, N., 2021. Increasing human-perceived heat stress risks exacerbated by urbanization in China: A comparative study based on multiple metrics. Earth's. Future 9(7), e2020EF001848. https://doi.org/10.1029/2020EF001848.
Luo, M., Lau, N., Liu, Z., Wu, S., Wang, X., 2022. An observational investigation of spatiotemporally contiguous heatwaves in China from a 3D perspective. Geophysical Research Letters 49. https://doi.org/10.1029/2022GL097714 e2022GL097714.
Luo, M., Ning, G., Xu, F., Wang, S., Liu, Z., Yang, Y., 2020. Observed heatwave changes in arid northwest China: Physical mechanism and long-term trend. Atmos. Res. 242, 105009 https://doi.org/10.1016/j.atmosres.2020.105009.
Ma H., Liu C., Qian Q., Xu, Z., Xiao, J., Yang, M., et al, 2020. Analysis on Climatic Characteristics of Extreme High-temperature in Zhejiang Province in May 2018 and Associated Large-scale Circulation. Journal of Arid Meteorology, 38(06): 909-919. https://doi.org/10. 11755/j.issn.1006-7639(2020)-06-0909.
Manning, C., Widmann, M., Bevacqua, E., van Loon, A.F., Maraun, D., Vrac, M., 2019. Increased probability of compound long-duration dry & hot events in Europe during summer (1950–2013). Environ. Res. Lett. 14 (9), 094006 https://doi.org/10.1088/1748-9326/ab23bf.
Mazdiyasni, O., AghaKouchak, A., 2015. Substantial increase in concurrent droughts and heatwaves in the United States. PNAS 112 (37), 11484–11489. https://doi.org/10.1073/pnas.1422945112.
Mukherjee, S., Mishra, A.K., 2020. Increase in Compound Drought and Heatwaves in a Warming World. Geophysical Research Letters, 48(1), e2020GL090617. https://doi.org/10.1029/2020GL090617.
Okabe, A., Satoh, T., Sugihara, K., 2009. A kernel density estimation method for networks, its computational method and a GIS-based tool. International Journal of Geographical Information Science 23 (1), 7–32. https://doi.org/10.1080/13658810802475491.
Rashid, M.M., Beecham, S., 2019. Development of a non-stationary Standardized Precipitation Index and its application to a South Australian climate. Sci. Total Environ. 657, 882–892. https://doi.org/10.1016/j.scitotenv.2018.12.052.
Ribeiro, A.F.S., Russo, A., Gouveia, C.M., Pires, C.A.L., 2020. Drought-related hot summers: A joint probability analysis in the Iberian Peninsula. Weather Clim. Extremes 30, 100279. https://doi.org/10.1016/j.wace.2020.100279.
Ridder, N.N., Pitman, A.J., Westra, S., Ukkola, A., Do, H.X., Bador, M., Hirsch, A.L., Evans, J.P., Di Luca, A., Zscheischler, J., 2020. Global hotspots for the occurrence of compound events. Nat. Commun. 11 (1) https://doi.org/10.1038/s41467-020-19639-3.
Sharma, S., Mujumdar, P., 2017. Increasing frequency and spatial extent of concurrent meteorological droughts and heatwaves in India. Sci. Rep. 7 (1), 15582. https://doi.org/10.1038/s41598-017-15896-3.
Shen, H., You, Q., Wang, P., Kong, L. 2018. Analysis on heat waves variation features in China during 1961-2014. Journal of the Meteorological Sciences, 2018, 38(1): 28-36. https://doi.org/10.3969 /2017jms.0026.
Shi, Z., Jia, G., Zhou, Y., Xu, X., Jiang, Y., 2021. Amplified intensity and duration of heatwaves by concurrent droughts in China. Atmos. Res. 261, 105743 https://doi.org/10.1016/j.atmosres.2021.105743.
Song, Z.Y., Xia, J., She, D.X., Zhang, L.P., Hu, C., Zhao, L., 2020. The development of a Nonstationary Standardized Precipitation Index using climate covariates: a case study in the middle and lower reaches of Yangtze River Basin. China. Journal of Hydrology 588, 125115. https://doi.org/10.1016/j.jhydrol.2020.125115.
Tegegne, G., Melesse, A.M., Worqlul, A.W., 2020. Development of multi-model ensemble approach for enhanced assessment of impacts of climate change on climate extremes. Sci. Total Environ. 704, 135357 https://doi.org/10.1016/j.scitotenv.2019.135357.
Trancoso, R., Syktus, J., Toombs, N., Ahrens, D., Wong, K.K.H., Pozza, R.D., 2020. Heatwaves intensification in Australia: A consistent trajectory across past, present and future. Sci. Total Environ. 742, 140521 https://doi.org/10.1016/j.scitotenv.2020.140521.
Vicente-Serrano, S.M., Begueria, S., Lopez-Moreno, J.I., 2010. A Multiscalar Drought Index Sensitive to Global Warming: The Standardized Precipitation Evapotranspiration Index. J. Clim. 23 (7), 1696–1718. https://doi.org/10.1175/2009JCLI2909.1.
Wang, Y., Chen, L., Song, Z., Huang, Z., Ge, E., Lin, L., Luo, M., 2018. Human-perceived temperature changes over South China: long term trends and urbanization effects. Atmos. Res. 215, 116–127. https://doi.org/10.1016/j.atmosres.2018.09.006.
Wang, D., You, Q.i., Jiang, Z., Wu, W., Jiang, Y., 2016. Analysis of extreme temperature changes in China based on the Homogeneity-Adjusted Data. Plateau Meteorology 35 (5), 1352–1363. https://doi.org/10.7522/j.issn.1000-0534.2016.00019.
Wang, W., Zhang, Y., Guo, B., Ji, M., Xu, Y., 2021. Compound Droughts and Heat Waves over the Huai River Basin of China: From a Perspective of the Magnitude Index. J. Hydrometeorol. 22 (11), 3107–3119. https://doi.org/10.1175/JHM-D-20-0305.1.
Wen, Q., Sun, P., Zhang, Q., 2020. A multi-scalar drought index for global warming: The non-stationary standardized precipitation evaporation index (NSPEI) and spatio-temporal patterns of future drought in China. Acta Geographica Sinica 75 (7), 1465–1482. https://doi.org/10.11821/dlxb202007010.
Wu, X., Hao, Z., Hao, F., Singh, V.P., Zhang, X., 2019. Dry-hot magnitude index: A joint indicator for compound event analysis. Environmental Research Letters, 14(6): https://doi.org/064017.10.1088/1748-9326/ab1ec7.
Wu, X., Wang, L., Yao, R., Luo, M., Wang, S., Wang, L., 2020. Quantitatively evaluating the effect of urbanization on heat waves in China. Sci. Total Environ. 731, 138857 https://doi.org/10.1016/j.scitotenv.2020.138857.
Xie, W., Zhou, B., You, Q., Zhang, Y., Ullah, S., 2020. Observed changes in heat waves with different severities in China during 1961–2015. Theor. Appl. Climatol. 141 (3–4), 1529–1540. https://doi.org/10.1007/s00704-020-03285-2.
Ye, D., Yin, J., Chen, Z., Zheng, Y., Wu, R., 2013. Spatiotemporal Change Characteristics of Summer Heatwaves in China in 1961–2010. Climate Change Research 9 (1), 15–20. https://doi.org/10.3969/j.issn.1673-1719.2013.01.003.
You, Q., Jiang, Z., Kong, L., Wu, Z., Bao, Y., Kang, S., Pepin, N., 2016. A comparison of heat wave climatologies and trends in China based on multiple definitions. Clim. Dyn. 48 (11–12), 3975–3989. https://doi.org/10.1007/s00382-016-3315-0.
Zambrano Mera, Y.E., Rivadeneira Vera, J.F., Angel Perez-Ma, M., 2018. Linking El Niño Southern Oscillation for early drought detection in tropical climates: The Ecuadorian coast. Sci. Total Environ. 643, 193–207. https://doi.org/10.1016/j.scitotenv.2018.06.160.
Zhang, Q., Singh, V.P., Li, J., Chen, X., 2011. Analysis of the periods of maximum consecutive wet days in China. Journal of Geophysical Research, 116, D23106, https://doi.org/10.1029/2011JD016088.
Zhang, W., Luo, M., Gao, Chen, S., W., Hari, V., Khouakhi, A., 2021b. Compound Hydrometeorological Extremes: Drivers, Mechanisms and Methods. Frontiers in Earth Science, 9: 673-495, https://doi.org/10.3389/feart.2021.673495.
Zhang, Y., Mao, G., Chen, C.,Chen, C., Shen, L., Xiao, B., 2021c. Population Exposure to Compound Droughts and Heatwaves in the Observations and ERA5 Reanalysis Data in the Gan River Basin, China. Land, 10(10),1021. https://doi.org/1021. 10.3390/land10101021.
Zhang, Y., Hao, Z., Feng, S., Zhang, X., Hao, F., 2022. Changes and driving factors of compound agricultural droughts and hot events in eastern China. Agric. Water Manag. 263, 107485 https://doi.org/10.1016/j.agwat.2022.107485.
Zhang, T., Su, X., Feng, K., 2021a. The development of a novel nonstationary meteorological and hydrological drought index using the climatic and anthropogenic indices as covariates. Sci. Total Environ. 786, 147385 https://doi.org/10.1016/j.scitotenv.2021.147385.
Zhang, Q., Zheng, Y., Singh, V.P., Luo, M., Xie, Z., 2017. Summer extreme precipitation in eastern China: Mechanisms and impacts. Journal of Geophysical Research: Atmospheres 122 (5), 2766–2778. https://doi.org/10.1002/2016jd025913.
Zheng, Y., Zhang, Q., Luo, M., Sun, P., Singh, V.P., 2019. Wintertime precipitation in eastern China and relation to the Madden-Julian oscillation: Spatiotemporal properties, impacts and causes. J. Hydrol. 582, 124477 https://doi.org/10.1016/j.jhydrol.2019.124477.
Zhou, N., Li, Y., Jia, X., 2021. Relationship between heavy precipitation and atmospheric wave with different time scales during Meiyu Period in Yangtze-Huai River Region. Journal of Tropical Meteorology 37 (1), 14–24. https://doi.org/10.16032/j.issn.1004-4965.2021.002.
Zscheischler, J., Westra, S., van den Hurk, B.J.J.M., Seneviratne, S.I., Ward, P.J., Pitman, A., AghaKouchak, A., Bresch, D.N., Leonard, M., Wahl, T., Zhang, X., 2018. Future climate risk from compound events. Nat. Clim. Change 8 (6), 469–477.